Photoelastic Visualisation _ Phased Array Sound Fields
Part 19 – Formation of grating lobes

Ed GINZEL [1]

[1] Materials Research Institute, Waterloo, Ontario, Canada
e-mail: eginzel@mri.on.ca
2014.12.15
Keywords: Photoelastic visualisation, ultrasonic, phased array
The video to this article can be seen here: www.ndt.net/search/docs.php3?id=16997&content=1

1. Introduction

This technical note is Part 19 of a series in NDT.net.

In Part 18 of this series, the formation of a basic 45° transverse plane wave was demonstrated. As the refracted angle is increased for a given probe and wedge combination, the conditions for the adjacent wavelets to form a beam by constructive interference deteriorate. The region within the beam for effective steering by phasal interference as described in text books [1], [2], is limited to the angle defined by the 6dB drop of the individual elements.

Although the user of a phased array system may configure the delay laws for a particular beam direction, the wavelets generated by the small elements are arcs that may have other points where constructive interference also occurs. When the interference in other regions is sufficiently pronounced, there can be lobes of pressure that are formed away from the intended direction of the beam. These are called grating lobes. Since these lobes can interact with the geometry and flaws in the same way as the main beam, the end result of grating lobes is to generate unwanted signals (artefacts). Steps are therefore used avoid the formation of grating lobes.

When using a linear array probe, the typical steps taken to avoid grating lobes include:

- Using lower frequency probes
- Increasing the damping of the elements to increase bandwidth of the wavelets
- Ensuring that the element pitch is less than half the nominal wavelength
- Reduce the angular sweep range used

The video associated with this article uses the same equipment setup as in Part 18. Since the 5L64 linear array probe has a pitch of only 0.6mm and the damping of the elements is relatively high resulting in a high bandwidth and the frequency is fixed. Therefore the only remaining variable of concern for grating lobes is just the angle of steering. The manufacturer recommends that the sweep range of the delay laws using this probe on the 36.5° refracting wedge be limited to ± 15° in order to avoid grating lobes. This would suggest that the angular sweep from the natural refracting angle (55°) be limited to 40°-70°. However, Civa modelling indicated that even at 74° no noticeable grating lobes would form.

In order to use this wedge and probe to demonstrate grating lobes it was therefore necessary to artificially adjust the element pitch. This was accomplished by using a 6 element delay law with every third element being activated.

Using every third element provides a pitch of 1.8mm which is significantly greater than the 0.5mm wavelength of the pulse in the cross-linked polystyrene wedge material.

The start element selected for the delay law was #10. Probe placement and activated elements are illustrated in Figure 1. The expected pressure pattern predicted by Civa is overlaid on the probe image in Figure 1.

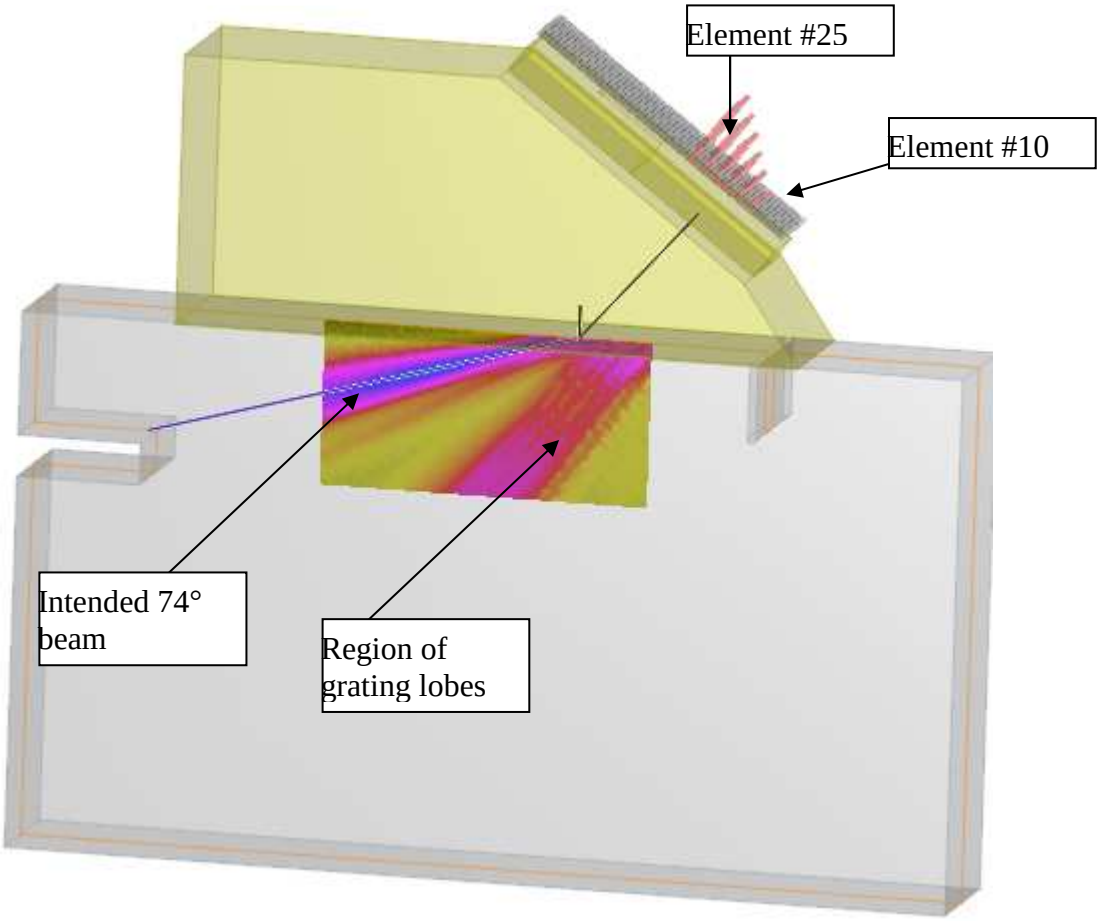

Figure 1 6 active element aperture with every third element activated from element #10 to #25 for a 74° refracted transverse plane wave

2. Comments on the Video

As with previous videos, a ruler is overlaid to allow assessment of the dimensions of features such as pulse wavelength. Towards the end of the video the ruler is replaced by a protractor to confirm the angle of the main beam (74°).

Evidence of the lower tip diffractions associated with the first two active elements is seen as an arc of compression mode entering the glass. This is the same arc shape seen in Part 14 of this series where we illustrated the individual element contributions to a wavefront formation. As a result of the large pitch, there is a pronounced arc associated with each element and the portion of the arc that strikes the wedge/glass interface at less than the first critical angle produces a similar arc in the glass. The first two such arcs are illustrated in Figure 2.

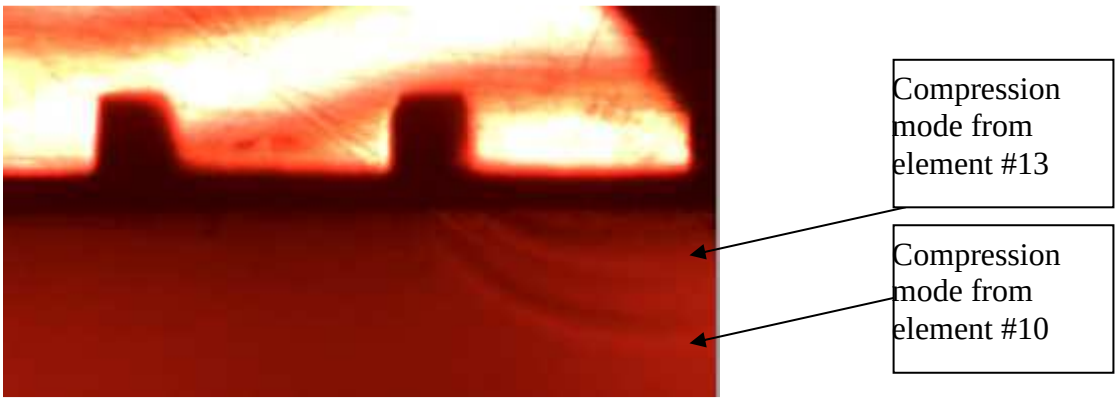

Figure 2 Compression mode arcs from the lower tip of elements #10 and #13

Eventually all the lower tip wavelets from the 6 activated elements move into the glass and the arc from each is seen separated from the bulk shear mode that forms the intended 74° beam. Figure 3 illustrates the 6 wavelets and also provides evidence for the transverse headwaves that form due to the glancing incidence of the compression mode wavelet at the glass/wedge interface.

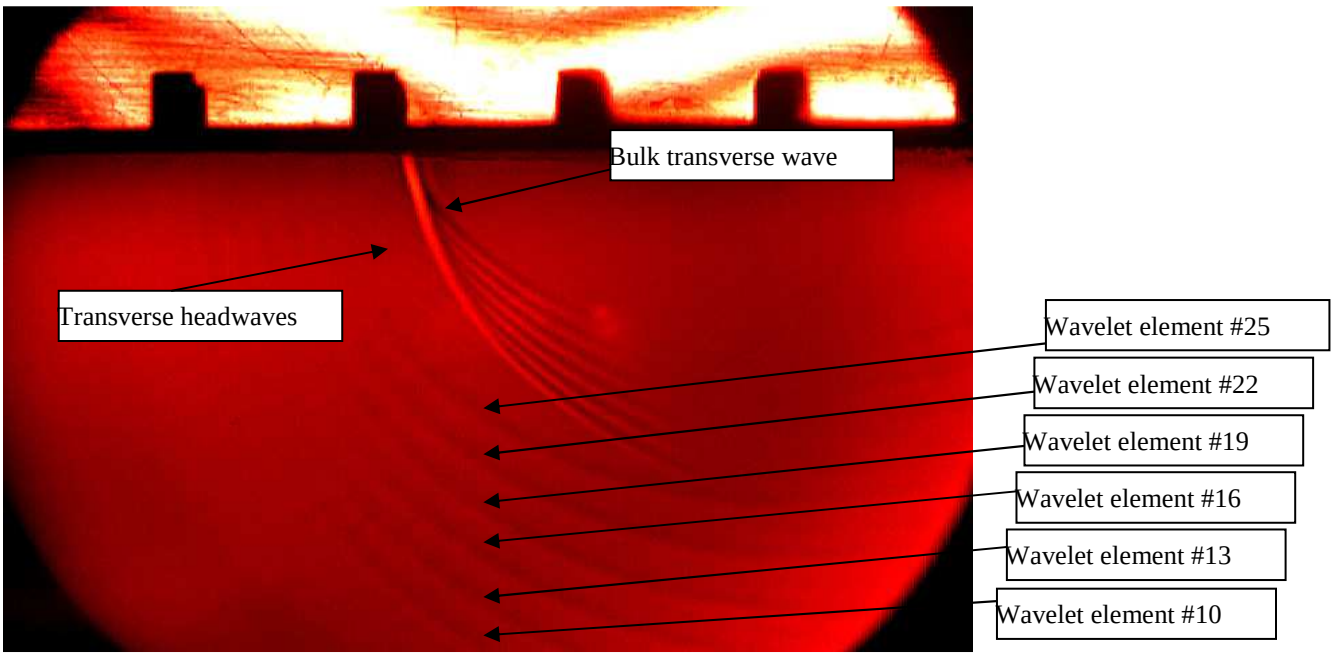

Figure 3 Wavelets, headwaves and bulk wave

Faint arcs of the transverse mode can also the seen moving off to the lower right. These are merely the result of mode conversion of the compression mode arcs.

Towards the end of the video we see the brightest portion of the transverse bulk wave pass through the region of the protractor confirming that a 74° beam was produced. This is illustrated in Figure 4.

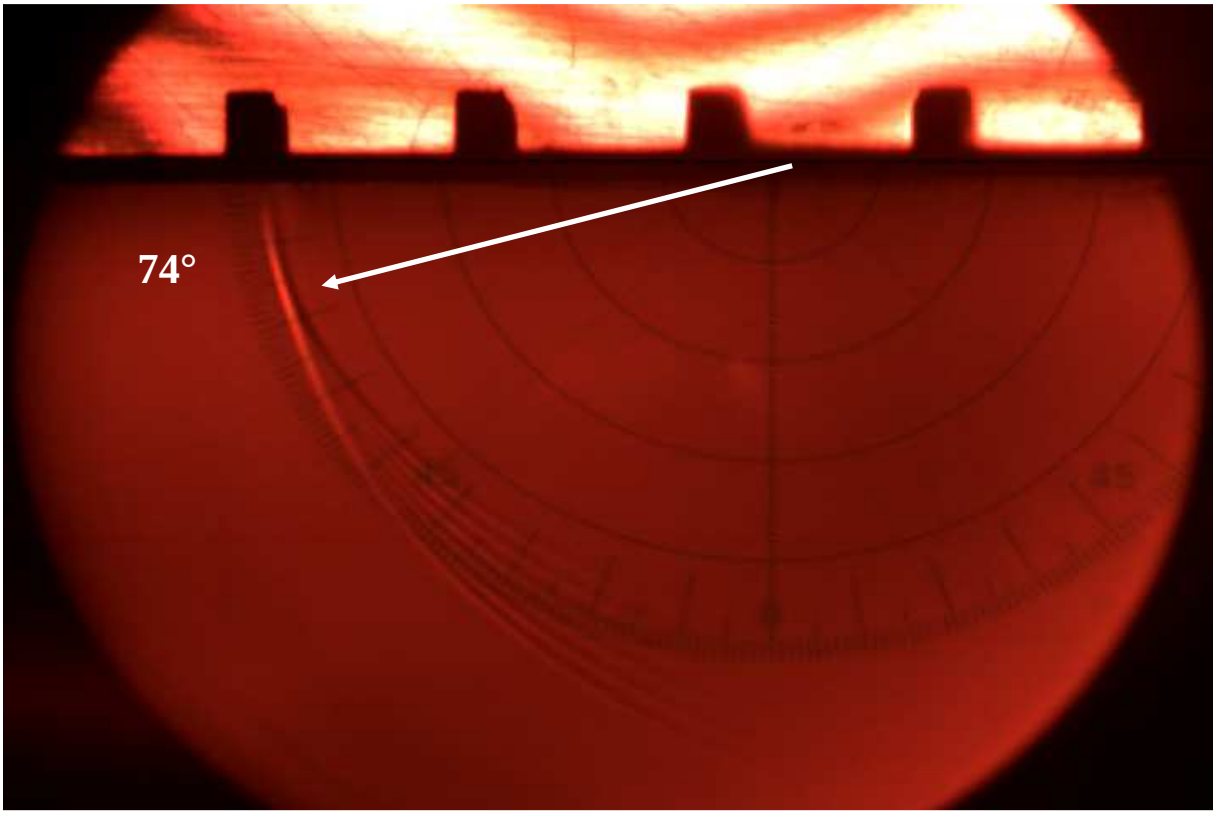

Figure 4 Confirming 74° refraction in glass

3. Description of Grating Lobe Formation

So now the reader may ask, "Where are the grating lobes?"

Simply watching the video provides no obvious indication of "lobes".
In order to see the grating lobes we must again return to the technique devised by Schmitte [3] whereby we add the brightest pixels in each frame of the video. Only then can the subtle variations that result due to constructive interference can be perceived.

Adding over 500 frames together and subtracting a reference frame by a technique called "dark frame subtraction" we can see the overall pattern of the beam progressing through the glass. The cumulative field with dark-field subtraction is seen in Figure 5. In Figure 5 we can actually see two forms of the grating lobes. One is the pattern of straight bands running at a slightly smaller angle than the 74° main beam. The other form of lobes can be seen as arcs that appear to have their centres at the point where the compression mode wavelets entered the glass.

In Figure 5 there is a dark line that arcs through the data. This is a result of a slight momentary increase in motion of the image (a bit like the loss of data when encoding a scan and the scanner makes a lurch when the wheel hits a small bump).

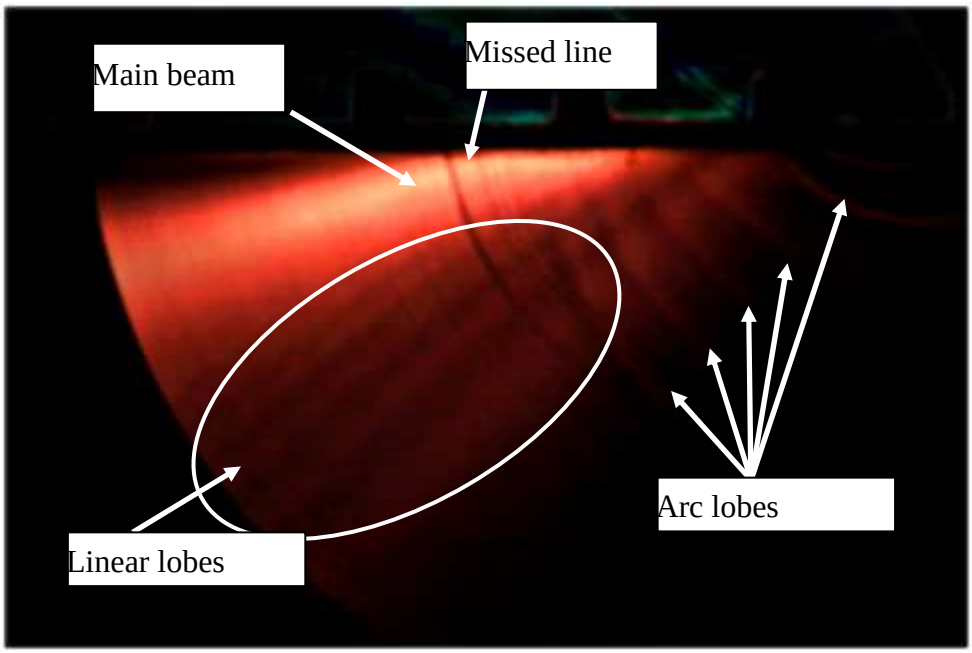

Figure 5 Accumulated frames with dark field subtraction

The pattern is easier seen when using an image rendering algorithm in the photoelastic software (IIA). This allows us to see that there are 5 linear lobes and 5 arc lobes as illustrated in Figure 6.

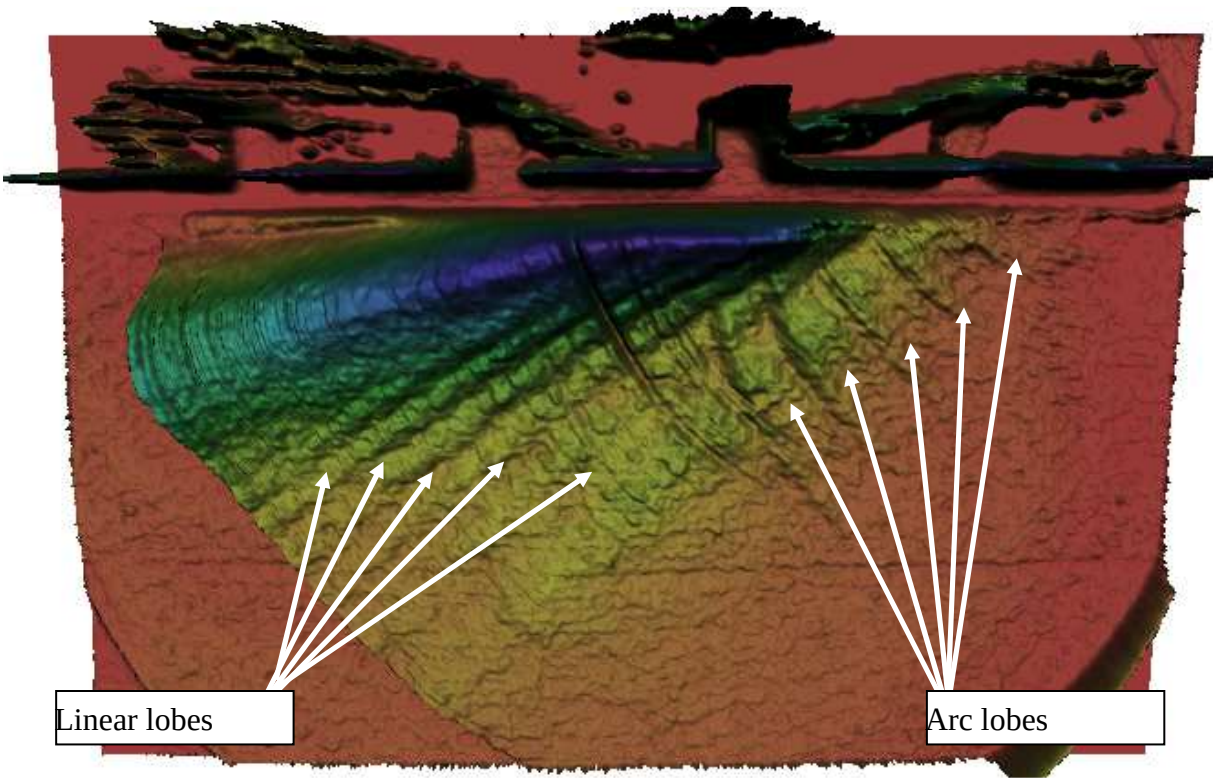

Figure 6 Rendered image to highlight lobe patterns

Figures 5 and 6 clearly illustrate the patterns, however, the process of formation is not so apparent and we must return to the video component frames to see how they form.

Linear bands form as the bulk transverse wave and its training diffraction arcs cross the head waves. The headwaves are formed by the compression mode arcs that have make glancing incidence along the glass/wedge interface.

Enhancing the image using embossing, we can see the location of the headwaves as they extend back and to the right. This places the headwaves in the path of the advancing arcs that have been formed from the mode conversion of the diffracted waves off the individual elements. The embossed enhancement image is seen in Figure 7.

As the arcs from the tails of the bulk transverse mode advance, the points available to interact with the headwave reduce to just the last arc of the group. This suggests that the bands of these linear grating lobes tend to narrow towards the main beam.

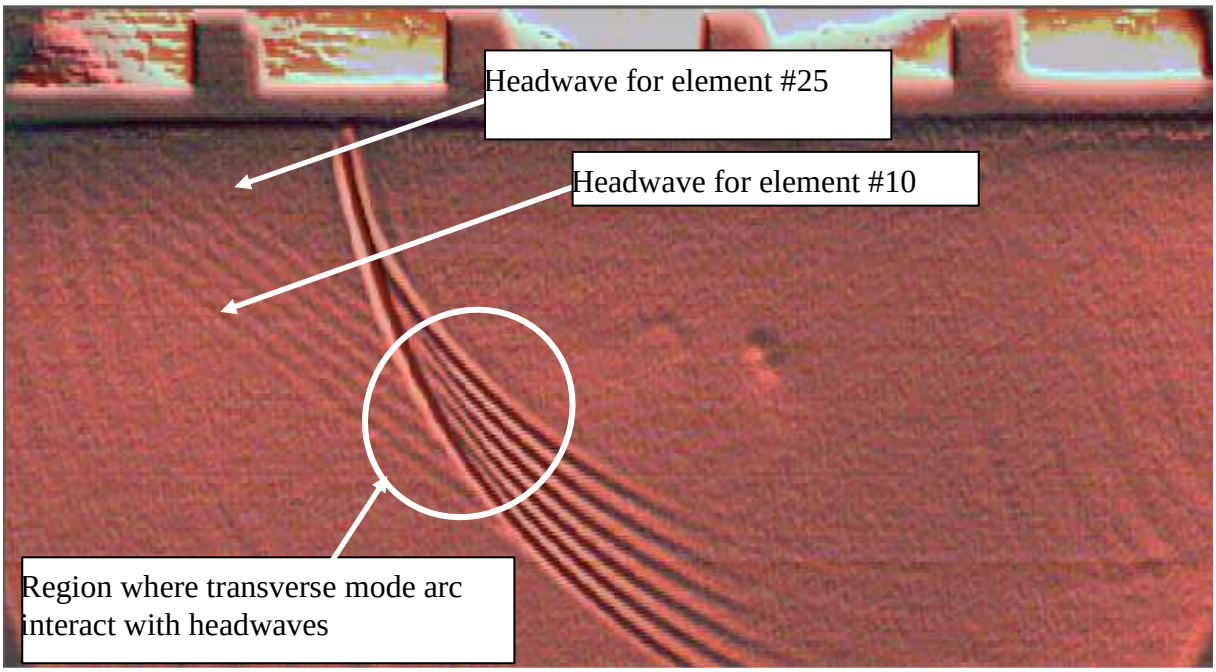

Figure 7 Identification of constructive interference points for the headwave and diffraction tail of the active elements

This suggests that regions of lobes formed by the interaction of the tail arcs and headwaves will have decreasing width for each wavelet. This appears to be substantiated in Figure 8.

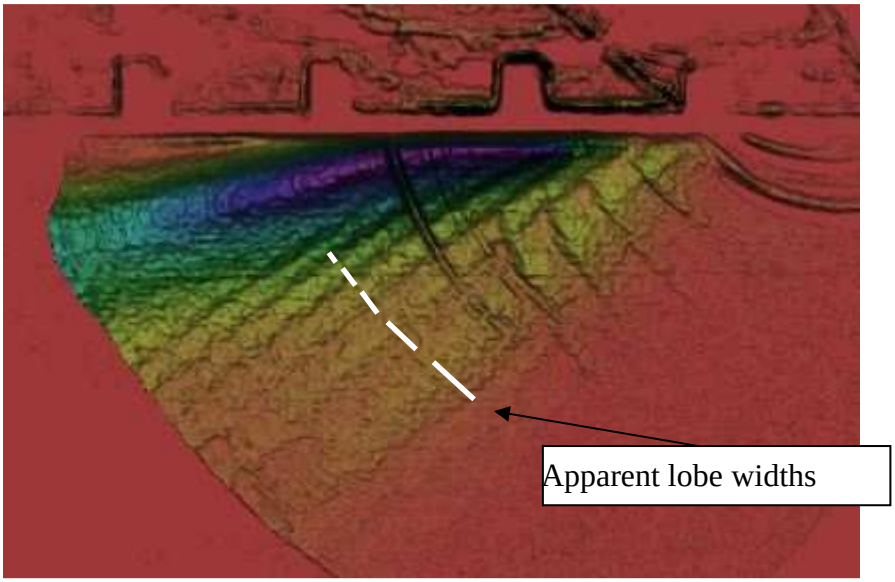

Figure 8 Decreasing width of lobes

Formation of the arc-shaped lobes relies on the constructive interference of the compression mode arc with the arc that also forms by the mode-converted transverse wave.

As the first arc enters the glass from the wavelet, it is in compression mode. However, at all points other than 0° incidence the compression mode will mode convert to transverse mode. This forms a second arc that lags the first. It is also the arc seen training the bulk transverse mode. The first wavelet in the glass and its associated transverse mode are seen in Figure 9.

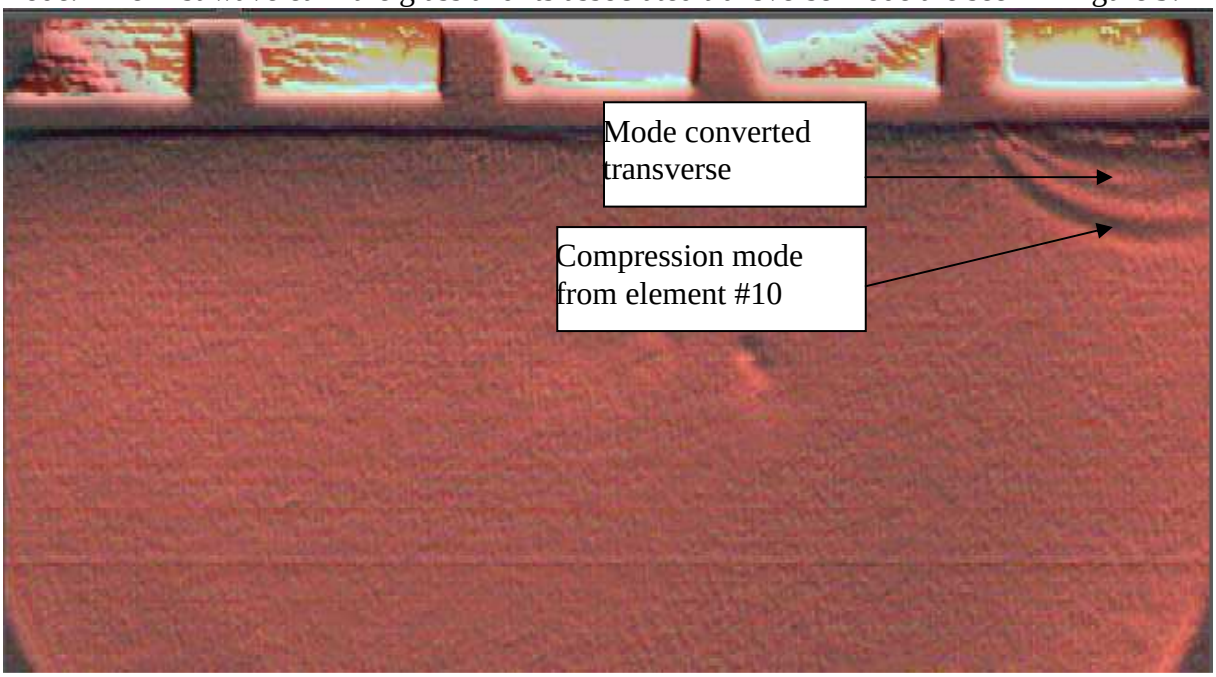

Figure 9 Formation of mode converted transverse wave from the initial compression mode arc

The arcs of constructive interference begin as the next compression mode wavelet enters, and then passes, the previously formed mode-converted transverse mode arc. This passing of the transverse arc by the second compression mode arc is illustrated in Figure 10.

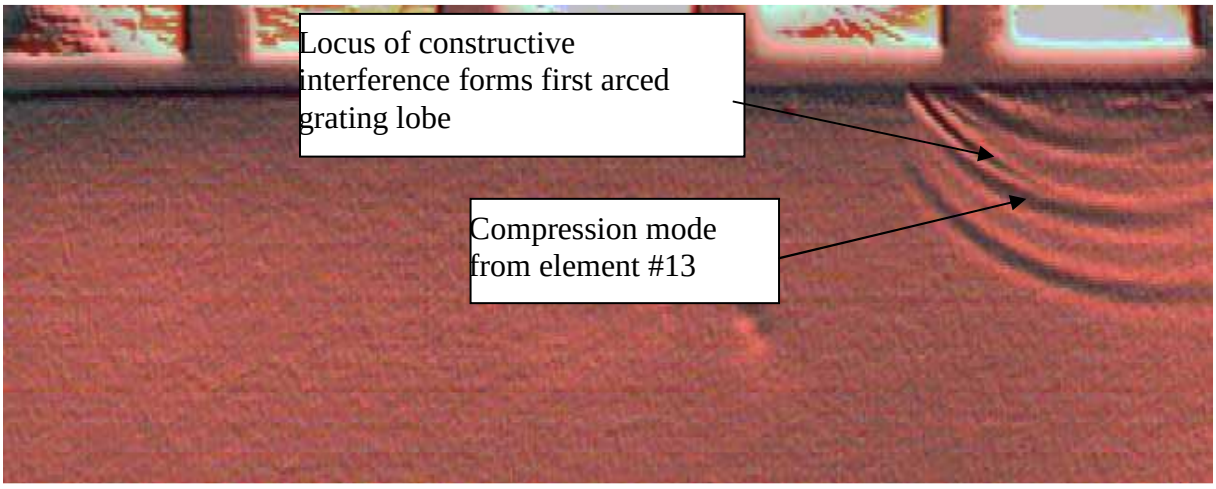

Figure 10 Constructive interference along mode converted transverse wave from the initial compression mode arc as second compression wavelet passes transverse wave

As the compression mode wavelets continue to enter the glass they gradually catch up to the earlier formed mode-converted transverse wave arcs. Figure 11 illustrates how the compression wave arc from the sixth wavelet to enter the glass catches up to the first and second arcs formed in transverse mode. The resultant arcs are the loci along the points where the two modes meet.

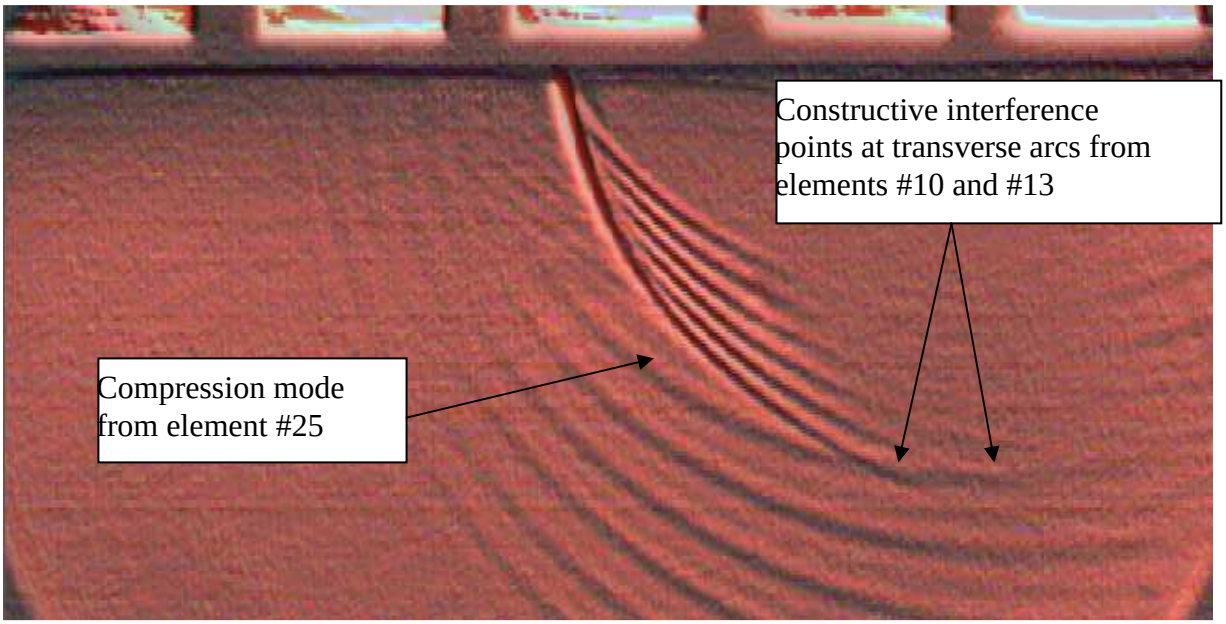

Figure 11 Points where the constructive interference from the compression mode of element #25 occurs along mode converted transverse wave arcs from elements #10 and #13

Using a high resolution simulation in Civa provides a clearer representation of both the linear and arc-shaped lobes. Figure 12 indicates three views of the photoelastic and Civa simulations.

The first view indicates the Civa B-scan of the beam overlaid on the rendered accumulated view and aligned with the main axis of the 74° beam. The main beam detail appears to be well matched between the Civa simulation and the photoelastic image.

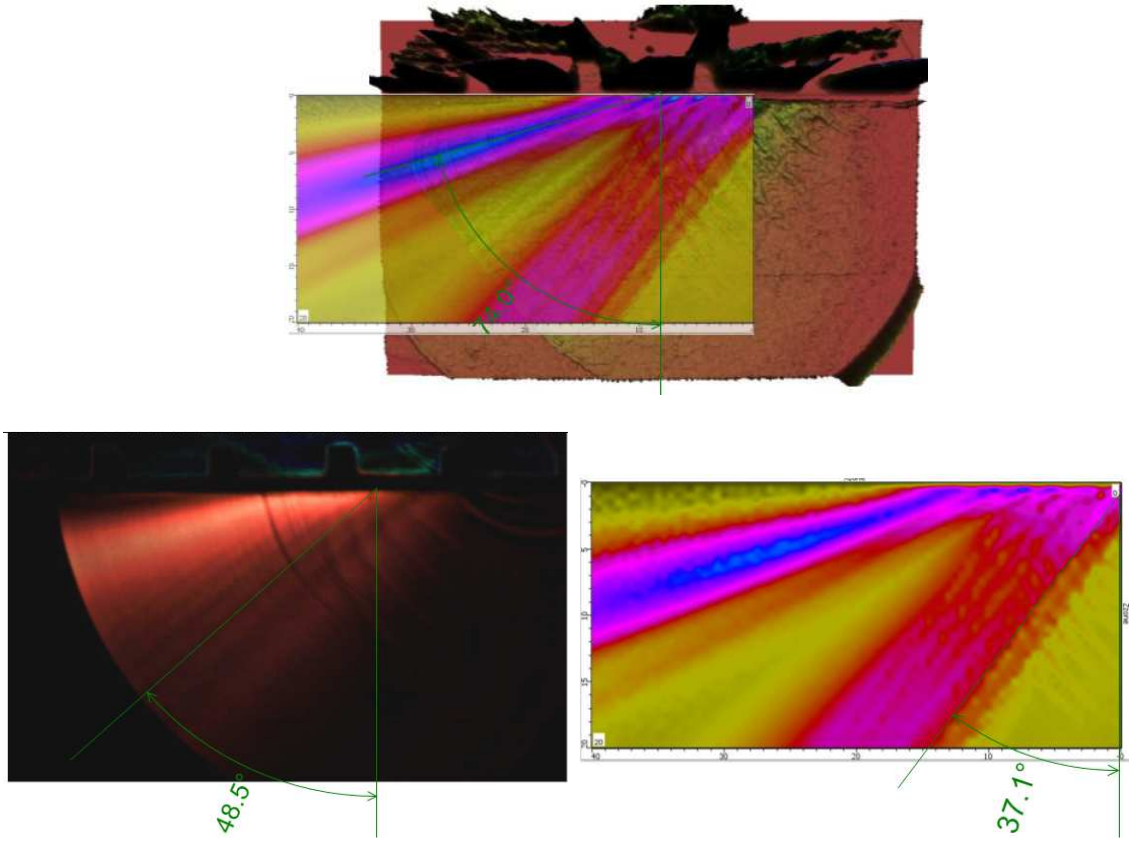

Figure 12 Comparing features of Civa simulation and Photoelastic image

Differences can be noticed between the simulation and photoelastic image. In the Civa simulation the linear lobes are clustered away from the main beam and have a general angle near 37°. This is very near the expected angle of the transverse headwave. In the photoelastic image the apparent angle of the linear lobes is near 48° and the lines are visible as parallel and extend across the region from where Civa indicates the group of 5 to occur and the photoelastic image indicates lines approaching the main beam. In the Civa image at least 9 arc-shaped lobes are indicated with a spacing nearly half that of the 5 arcs seen in the photoelastic image.

Using an overlay of the line connecting the intersection point of the leading diffraction edge as it intersects with the headwave generated by element #13, we see that the interference points trace a line with an angle near 48° as indicated in Figure 13.

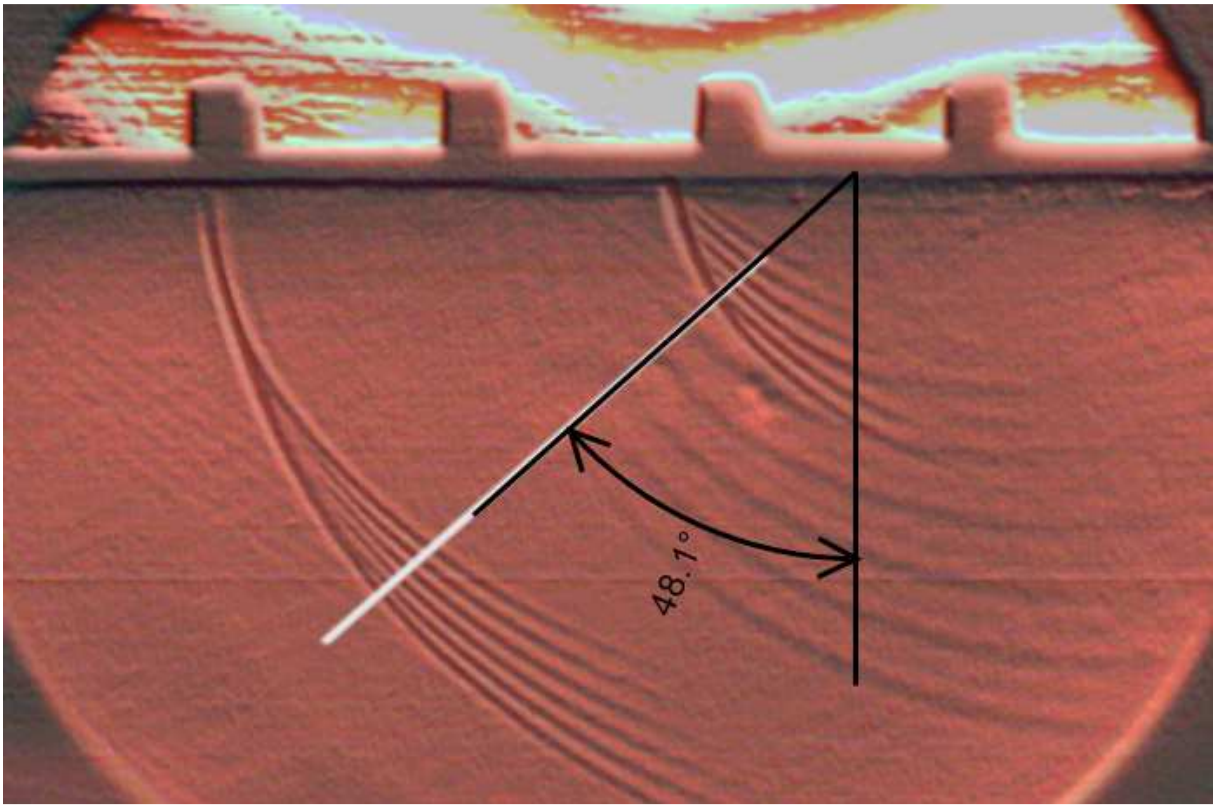

Figure 13 Origin of 48° line of interference using element #13 headwave and main diffraction curve (2 video frames merged to indicate positions at two points in time)

4. Comparing Intensities

To illustrate the effect that might be seen by the operator, image captures are made of the peaked signals from the main lobe and grating lobe on the 5mm diameter hole in the glass sample. These are compared in Figures 14 and 15.

Whereas the main beam has a relatively sharp peak on the A-scan, the grating lobe effect has a series of peaks over a range of approximately 2mm equivalent depth. The multiple peaks correspond to the curved diffraction components seen in the main linear grating lobe.

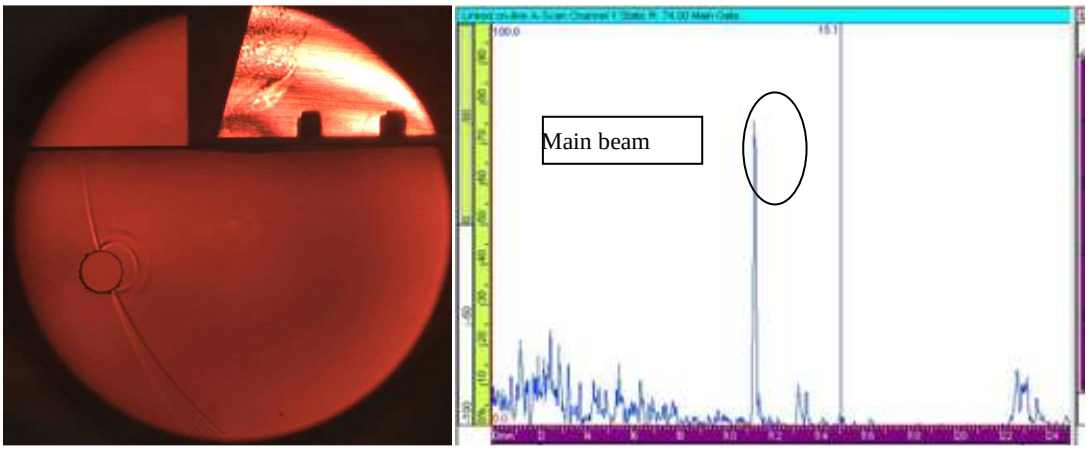

Figure 14 Main beam peaked on 5mm SDH and associated A-scan

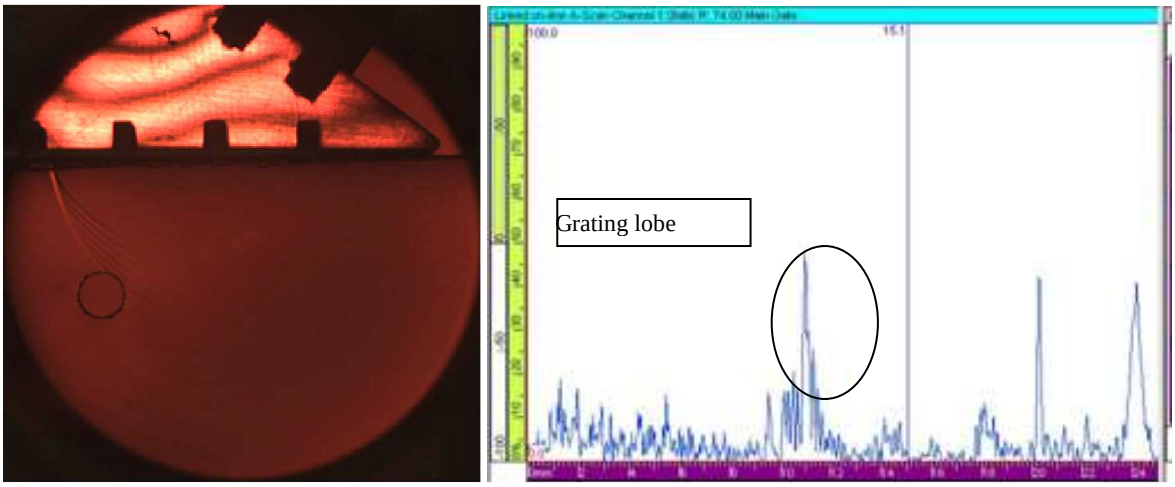

Figure 15 Maximised grating lobe peaked on 5mm SDH and associated A-scan

The maximum amplitude of the main beam was set to about 80% screen height and then the probe moved forward to locate the maximum amplitude of the grating lobe region. This produced a signal near 45% screen height or about 5dB lower than the main beam.

Comparing the relative amplitudes by using the echo-dynamic tool in Civa and the image intensity plot in the IIA software of the photoelastic system, we see similar apportioning of the amplitudes (see Figure 16). Civa indicates 5.9dB drop and IIA indicates about 6dB drop (assessment in Civa and IIA are made at about 9mm depth because the image plotting does not extend to the same depth (12mm) as the 5mm SDH.

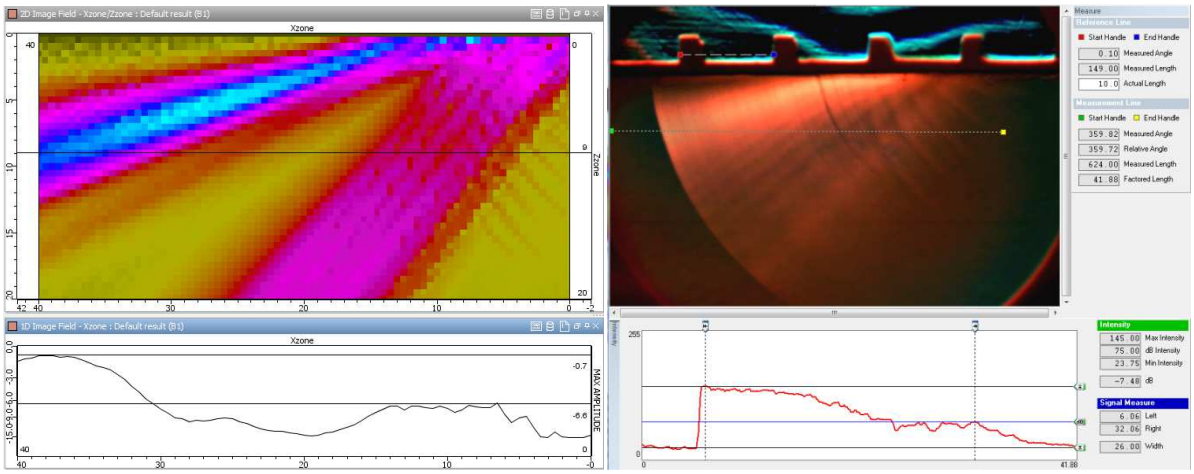

Figure 16 Comparing Civa and IIA amplitude drops

For more information about the photoelastic system see
http://eclipsescientific.com/Products/Training/Photoelastic/index.html
For information on the Image Intensity Analysis software see
http://eclipsescientific.com/Software/IIA/info.html

References

1. Phased Array Ultrasonic Technology- 2nd Edition, E. Ginzel; Publisher Eclipse Scientific, 2013
2. Introduction to Phased Array Ultrasonic Technology Applications: R/D Tech Guideline, Publisher ONDT, 2004
3. Till SCHMITTE, Thomas ORTH, Martin SPIES, Thomas KERSTING, Schallfelder von Phased-Array Prüköpfen: Vergleich von photoelastischen Messungen und Simulationen, http://www.ndt.net/article/dgzfp2012/papers/di2a1.pdf, NDT.net, 2012

The video to this article can be seen here: www.ndt.net/search/docs.php3?id=16997&content=1